Nucl Med Mol Imaging (2014) 48:47–54
DOI 10.1007/s13139-013-0241-5

ORIGINAL ARTICLE

Automated Analysis of ^{123}I-beta-CIT SPECT Images with Statistical Probabilistic Anatomical Mapping

Jae Seon Eo · Ho-Young Lee · Jae Sung Lee · Yu Kyung Kim · Bum-Seok Jeon · Dong Soo Lee

Received: 27 March 2013 / Revised: 28 August 2013 / Accepted: 2 October 2013 / Published online: 6 November 2013

Abstract
Background Population-based statistical probabilistic anatomical maps have been used to generate probabilistic volumes of interest for analyzing perfusion and metabolic brain imaging. We investigated the feasibility of automated analysis for dopamine transporter images using this technique and evaluated striatal binding potentials in Parkinson's disease and Wilson's disease.
Materials and Methods We analyzed 2β-Carbomethoxy-3β-(4-^{123}I-iodophenyl)tropane (^{123}I-beta-CIT) SPECT images acquired from 26 people with Parkinson's disease (M:F=11:15, mean age=49±12 years), 9 people with Wilson's disease (M: F=6:3, mean age=26±11 years) and 17 normal controls (M:F=5:12, mean age=39±16 years). A SPECT template was created using striatal statistical probabilistic map images. All images were spatially normalized onto the template, and probability-weighted regional counts in striatal structures were estimated. The binding potential was calculated using the ratio of specific and nonspecific binding activities at equilibrium. Voxel-based comparisons between groups were also performed using statistical parametric mapping.
Results Qualitative assessment showed that spatial normalizations of the SPECT images were successful for all images. The striatal binding potentials of participants with Parkinson's disease and Wilson's disease were significantly lower than those of normal controls. Statistical parametric mapping analysis found statistically significant differences only in striatal regions in both disease groups compared to controls.
Conclusion We successfully evaluated the regional ^{123}I-beta-CIT distribution using the SPECT template and probabilistic map data automatically. This procedure allows an objective and quantitative comparison of the binding potential, which in this case showed a significantly decreased binding potential in the striata of patients with Parkinson's disease or Wilson's disease.

Keywords Automated analysis · Statistical probabilistic anatomical mapping · Parkinson's disease · Wilson's disease · ^{123}I-beta-CIT

Jae Sung Lee and Dong Soo Lee contributed equally to this work.

This article is Jae Seon Eo's master's thesis.

J. S. Eo · J. S. Lee (✉) · Y. K. Kim · D. S. Lee (✉)
Department of Nuclear Medicine, Seoul National University College of Medicine, 101 Daehang-ro, Jongro-gu, Seoul 110-744, Korea
e-mail: jaes@snu.ac.kr
e-mail: dsl@snu.ac.kr

J. S. Eo
Department of Nuclear Medicine, Korea University Anam Hospital, Seoul, Korea

H.-Y. Lee
Department of Nuclear Medicine, Seoul National University Bundang Hospital, Gyeonggi-do, Korea

Y. K. Kim
Department of Nuclear Medicine, Boramae Medical Center, Seoul, Korea

B.-S. Jeon
Department of Neurology, Seoul National University College of Medicine, Seoul, Korea

D. S. Lee
Department of Molecular Medicine and Biopharmaceutical Sciences, Seoul National University, Seoul, Korea

Introduction

Quantifiability is a major advantage of nuclear medicine imaging, which yields images of great clinical value. Because small errors in regions of interest (ROIs) can result in large discrepancies, generating ROIs is very important for quantitative analysis. Such errors can occur

Table 1 Subject characteristics

		Disease	Controls	*t*-test
PD	Age	49.2±12.0	47.3±12.0	NS
	M:F	11:15	3:8	
WD	Age	26.1±11.2	30.7±8.5	NS
	M:F	6:3	4:5	

PD Parkinson's disease, *WD* Wilson's disease, *NS* not significant

with manual drawing of the ROI. Furthermore, ROI values can vary between the manual drawing and setting of the ROI.

Evolving computer technology has developed advanced image-matching and transformation techniques such as voxel-based comparison with statistical parametric mapping (SPM) and a population-based probabilistic brain atlas called a "statistical probabilistic anatomical map" (SPAM) [1]. The user can easily designate the volume of interest (VOI) with such a standardized brain map, minimizing interpersonal variation and maximizing the reproducibility with SPAM. These SPM and SPAM techniques have been applied to several kinds of brain imaging analysis including dopamine receptor imaging [2–6].

Parkinson's disease (PD) and Wilson's disease (WD) are neurodegenerative disorders that primarily affect the striatal area of the midbrain. Therefore, dopamine transporter ligand images can be helpful for diagnosing PD and WD. 2β-Carbomethoxy-3β-(4-^{123}I-iodophenyl)tropane (^{123}I-beta-CIT) is one of the radiopharmaceuticals for dopamine transporter imaging that is suitable for single-photon emission computed tomography (SPECT) [7].

In this study, we investigated the feasibility of automatic analysis of dopamine transporter images using the SPAM technique and evaluated the striatal binding potential in patients with PD and WD.

Materials and Methods

Subjects

From 1996 to 2002, we retrospectively analyzed the ^{123}I-beta-CIT SPECT brain images of 26 people with PD, 9 people with WD, and 17 normal controls. The protocol was approved by the local institutional review board, and patient consent was not required because of the retrospective nature of the study. The mean age of the 26 participants with PD (15 women and 11 men) was 49.2±12.0 years. These participants with three or more classical PD symptom including resting tremor, postural instability, rigidity, and bradykinesia had been clinically diagnosed by a neurologist. The mean age of the nine participants with WD (3 women and 6 men) was 26.1± 11.9 years. Neurologists confirmed the diagnosis by an appropriate history of neurological impairment, low serum ceruloplasmin concentration, low serum copper concentration, increased urinary copper excretion, and Kayser-Fleischer rings. All participants had Parkinsonian symptoms and dystonia as neurological manifestations of WD. The average age of the 17 normal controls (12 women and 5 men) was 38.8±16.0 years. None of them had a history of neuropsychiatric disease or signs of neurological impairment, which was confirmed by neurologists.

To control for age-related changes in neurological status, we selected 11 age-matched normal controls for participants with PD (8 women and 3 men, mean age 49.2±12.0 years) and 9 for participants with WD (5 women and 4 men, mean age 30.7±8.5 years). There was no significant difference in mean age between participants with PD or WD and normal controls (Table 1).

^{123}I-beta-CIT SPECT Acquisition and Reconstruction

In participants with PD, antiparkinsonian medications were stopped for 48 h prior to image acquisition. All participants

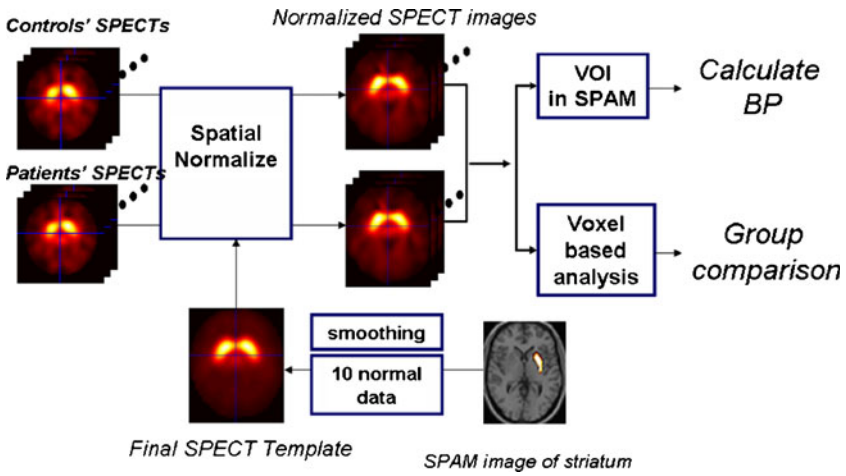

Fig. 1 Automated analysis method. This figure shows a schematic diagram for constructing the SPECT template, normalizing images, calculating the binding potential, and comparing the control and disease groups

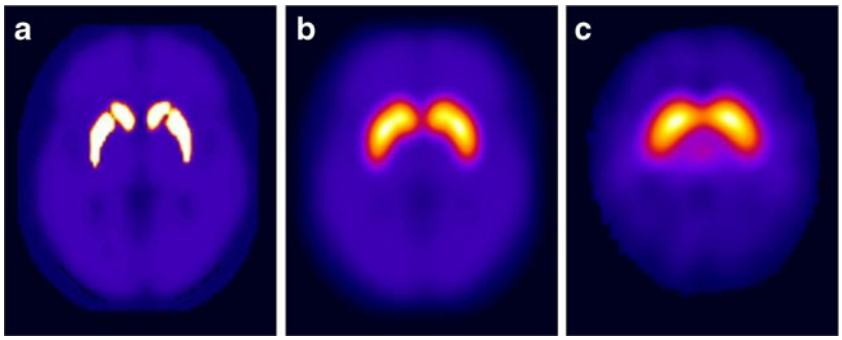

Fig. 2 Construction of the ^{123}I-beta-CIT SPECT template. (**a**) Initial striatal template consists of caudate and putamen. (**b**) Ideal SPECT model of ^{123}I-beta-CIT distribution. (**c**) Average image of 10 control subjects spatially normalized on image (**b**): This image was used for the final template for SPM and SPAM analysis

with WD were taking penicillamine. No participants were taking dopaminergic medications for their neurological symptoms. Five percent Lugol's solution of elemental iodine and potassium iodide (total 450 mg iodine) was orally administered to all participants 1 day before the SPECT study. A bolus injection of ^{123}I-beta-CIT 370 MBq was performed over 30 s. SPECT studies were performed using a triple-headed gamma camera (Prism 3000, Picker, USA) equipped with a medium energy collimator. Scans were obtained 18 h after radioactive material injection. Data were acquired with a 20 % symmetric window centered at 159 keV using a 128×128 matrix (pixel size 4.67×4.67 mm, slice thickness 4.67 mm) and reconstructed by filtered back projection with a Butterworth filter (cutoff 0.4 cycle/cm, order 7). Chang's method of attenuation correction (μ 0.1/cm) was employed.

SPM Analysis

SPM99 (statistical parametric mapping, University Collage of London, UK) and Matlab 6.5 (Mathwork Inc., USA) software was used for spatial matching and statistical analysis. We developed a standard anatomical brain template for dopamine receptor and transporter images using SPAM. In this study, as we did not have 3D MRI brain images, we used SPAM to create the standard template using the following sequence (Figs. 1 and 2).

(1) Create whole-head images by binary-coding selected SPM-provided proton density-weighted MR images with pixel values greater than 5,000.
(2) Create whole-brain images by summing the gray matter and white matter SPAM templates.

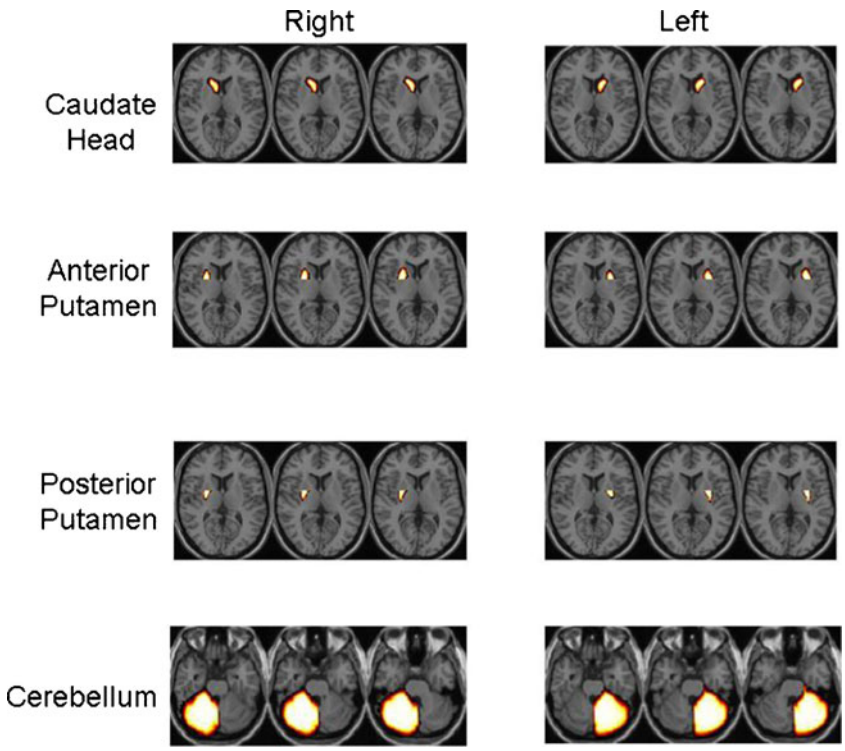

Fig. 3 MNI template of the caudate head, anterior putamen, posterior putamen, and cerebellum

Table 2 Brain areas with significantly decreased uptake in participants with Parkinson's disease compared to controls (FDR corrected, $p<0.05$, K>50)

Regions included in cluster	Coordinates (x, y, z)	Peak Z-value	p-value (FDR corrected)
Right posterior putamen	32, 2, −4	4.97	0.001
Left posterior putamen	−30, 0, −6	4.92	0.001
Right anterior putamen	14, 16, 2	4.75	0.001
Left anterior putamen	−14, 12, 2	4.55	0.001
Right caudate	16, 22, −2	4.10	0.001
Left caudate	−12. 26. −4	4.45	0.001

FDR false discovery rate

Table 3 Brain areas with significantly decreased uptake in participants with Wilson's disease compared to controls (FDR corrected, $p<0.05$, K>50)

Regions included in cluster	Coordinates (x, y, z)	Peak Z-value	p-value (FDR corrected)
Right posterior putamen	32, 4, −12	3.62	0.007
Left posterior putamen	−28, −4, −16	4.39	0.002
Right anterior putamen	26, 14, −14	5.83	<0.001
Left anterior putamen	−18, 12, −18	4.62	0.002
Right caudate	12, 16, 4	3.96	0.004
Left caudate	−8, 20, 2	4.07	0.004

FDR false discovery rate

(3) Create SPAM of the striatum by summing the caudate and putamen SPAM templates.
(4) Set weight parameters according to normal controls' ^{123}I-beta-CIT count ratios after smoothing with a 12-mm Gaussian kernel (ratios listed below):

Specific binding area: nonspecific binding area: peripheral non-brain area=10:1:0.5.

(5) Sum the SPAM images of the striatium, brain (whole brain image, WBI), and head (whole head image, WHI) and multiply by the following weight parameters:

$$0.5 \times \mathrm{WHI} + 0.5 \times \mathrm{WBI} + 9.0 \times \mathrm{Striatum}.$$

(6) Create the initial template after smoothing the summed image with a 12-mm Gaussian kernel to be made equal to the resolution of the SPECT image.
(7) Create the final standard template by averaging the SPECT images of ten normal controls that were spatially normalized to the initial template and count-normalized to the cerebellum.

All participants' ^{123}I-beta-CIT SPECT images were spatially normalized to the standard template using affine and nonlinear transformation and count-normalized to the cerebellum.

Analyses of covariate tests in SPM were performed with age covariation to elucidate differences between participants with PD or WD and normal controls. The error due to multiple comparisons was corrected with the false discovery rate (FDR) regulation method. P-values less than 0.05 were considered to be significant. An accumulated mass of more than 50 contiguous voxels was defined as a significantly different area.

Analysis and Quantification of Binding Potential with SPAM

Spatial- and count-normalized images were subdivided into probabilistic ROIs with the Montreal Neurological Institute (MNI) SPAM template. Each voxel of SPAM has the probability (0 to 1) of belonging to 98 ROIs that comprise the MNI template. The ROI count can be measured as a probability-weighted mean count, defined as the sum of voxel counts multiplied by the voxel probability of the brain ROI. With this quantification method using SPAM, the probability-weighted mean counts were measured in the caudate head, anterior putamen, posterior putamen, and cerebellum as a non-specific binding area (Fig. 3).

The binding potential is defined as the specific-nonspecific uptake ratio at equilibrium. We defined the specific uptake areas as the caudate head, anterior putamen, and posterior putamen. We defined the nonspecific uptake area as the cerebellum. The binding potential (BP) was calculated using the following formula:

$$\mathrm{BP} = (\text{count per pixel of specific binding areas} / \text{count per pixel of nonspecific binding areas}) - 1$$

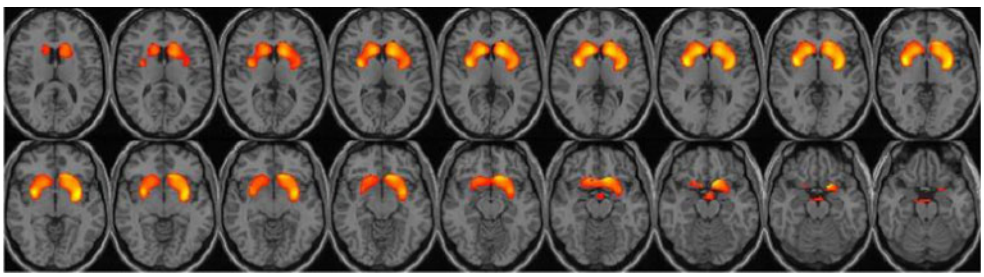

Fig. 4 SPM result: voxel-based comparison between controls and participants with Parkinson's disease. †Age covariate, FDR-corrected $p<0.05$, cluster 50

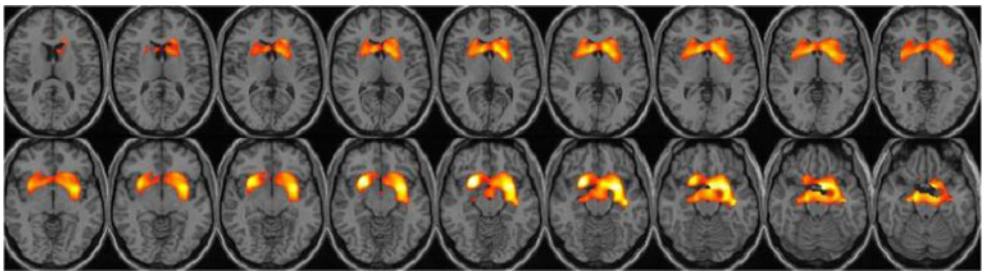

Fig. 5 SPM result: voxel-based comparison between normal controls and participants with Wilson's disease. †Age covariate, FDR-corrected $p<0.05$, cluster 50

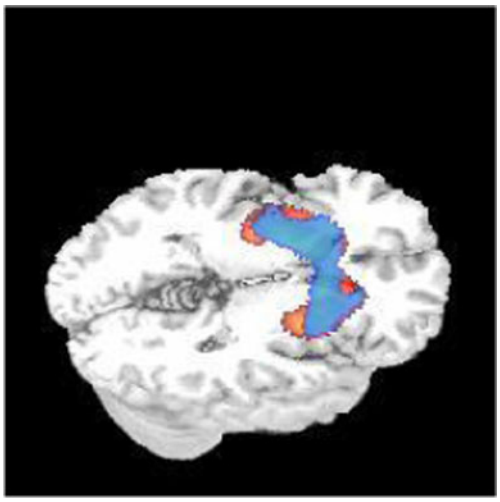

Fig. 6 SPM result comparison between participants with Parkinson's disease and Wilson's disease. *Blue area* is significantly decreased area in Wilson's disease and red area is significantly decreased area in Parkinson's disease compared to controls

Binding potential measurements were performed twice in all study participants by a single observer using the same method; measurements were compared to test for reproducibility. To compare the reduction in binding potential area between participants with PD and those with WD, the Z-score of each area was calculated as follows:

$$\text{Z-score} = (\text{BP of participants with PD or WD} - \text{mean BP of controls}) / \text{standard deviation of control BP}$$

Statistical Analysis

We compared the binding potential between disease groups and controls using the general linear model with age covariation. We used the Bonferroni correction to make multiple binding potential comparisons of the six ROIs (bilateral caudate heads, anterior putamina, and posterior putamina). We used paired t-tests to compare Z-scores between groups.

Results

SPM Analysis

Using SPM99 software, we found significant differences between the binding potentials of the disease group's volumetric areas and those of the control groups. In participants with PD, binding potentials were significantly lower than those of normal controls in the bilateral caudate heads, anterior putamina, and posterior putamina (Table 2). This area of decreased binding potential can be represented by the whole striatum (Fig. 4). Similarly, in participants with WD, binding potentials were also significantly lower than those of normal controls in bilateral caudate heads, anterior putamina, and posterior putamina (Table 3). Again, this area

Table 4 Binding potentials acquired by SPAM-assisted VOI methods in control versus disease groups

Regions	Parkinson's disease		Wilson's disease	
	Controls	Disease	Controls	Disease
Left caudate head	5.95±0.44	4.39±1.1**	6.41±0.37	5.18±0.92**
Right caudate head	5.71±0.53	4.32±1.01**	6.08±0.42	4.96±0.77**
Left anterior putamen	6.29±0.39	4.67±1.16**	6.71±0.34	5.5 ±0.87**
Right anterior putamen	6.06±0.52	4.47±1.15**	6.39±0.45	5.2 ±0.78**
Left posterior putamen	4.25±0.21	3.32±0.73**	4.48±0.15	3.83±0.62**
Right posterior putamen	3.64±0.29	2.8 ±0.69**	3.74±0.18	3.45±0.58**

** $p<0.005$

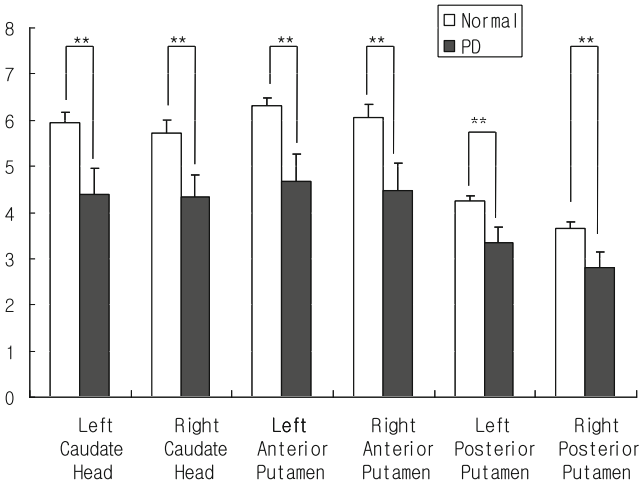

Fig. 7 Binding potentials in controls and in participants with Parkinson's disease. †Global linear model, age covariate, corrected for multiple comparisons $^{**}p<0.005$

of decreased binding potential can be represented by the whole striatum (Fig. 5). When comparing disease groups, the binding potentials of the posterior putamen were significantly decreased in participants with PD compared to those of participants with WD (Fig. 6).

Quantification of Binding Potential Using SPAM

Our automated method successfully obtained the binding potentials of the caudate, anterior putamen, and posterior putamen from all study participants (Table 4). In participants with PD, the binding potentials of all striatal areas were significantly lower than those of normal controls (Fig. 7). Similarly, the striatal binding potentials of participants with WD were also significantly lower than those of normal controls (Fig. 8).

In participants with PD, the regional Z-score of the binding potential in the caudate was −3.09, significantly different from those of the anterior putamen (−3.57) and posterior putamen (−3.61) ($p<0.005$). In participants with WD, however, the regional Z-scores of the caudate, anterior putamen, and posterior putamen were −3.00, −3.09, and −3.00, values that are not significantly different from each other ($p> 0.690$) (Fig. 9).

Discussion

Recently, many clinical and experimental trials of dopamine receptor imaging have been performed [8–10]. In this study, we normalized ^{123}I-beta-CIT images using SPAM in terms of shape and count and obtained binding potentials using an automated method. It is known that striatal uptake of ^{123}I-beta-CIT decreases with age [11]. Given that the mean age of participants in the disease group was significantly different from the mean age of controls, we created age-matched normal control groups for each disease group (PD and WD). In line with previous reports, SPM analysis found that striatal uptake was significantly lower in patients with PD or WD compared to normal controls (Figs. 4–5) [7, 12, 13].

Although PD and WD cause similar Parkinsonian motor symptoms, there are differences in both the pathophysiology and visual ^{123}I-beta-CIT SPECT images of patients with the disease [7]. Our SPM analysis showed differences in uptake in the posterior putamen between participants with PD and those with WD (Fig. 6). Therefore, we measured the individual binding potentials of different striatal regions using VOIs of SPAM.

We used SPAM of the caudate, anterior putamen, posterior putamen, and cerebellum as VOIs. The occipital lobe is also commonly used as a non-specific uptake region of reference in such studies. In this study, however, we used the cerebellum as the region of reference because we found that individual variations in occipital uptake were higher than variations in cerebellar uptake.

In this study, we found that the binding potentials of all striatal regions (caudate, anterior putamen, posterior putamen) in participants with PD or WD were significantly lower than those of normal controls. In a Z-score comparison, the binding potentials of the putamen in participants with PD were more significantly decreased than those of the caudate. This difference between Z-scores of the caudate and putamen was negligible in participants with WD. This result suggests that posterior striatum (putamen) involvement preceded the involvement of other striatal regions in PD [14].

In WD, the reductions in binding potential were not significantly different in the caudate, anterior putamen, or posterior putamen. In contrast, a previous study found significant differences in binding potential reduction between the caudate and putamen [12]. This discrepancy may be due to the small number of participants in our study.

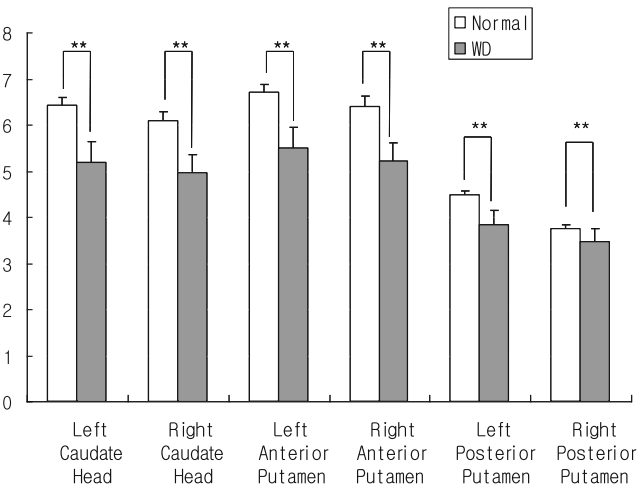

Fig. 8 Binding potentials in controls and participants with Wilson's disease. †Global linear model, age covariate, corrected for multiple comparisons $^{**}p<0.005$

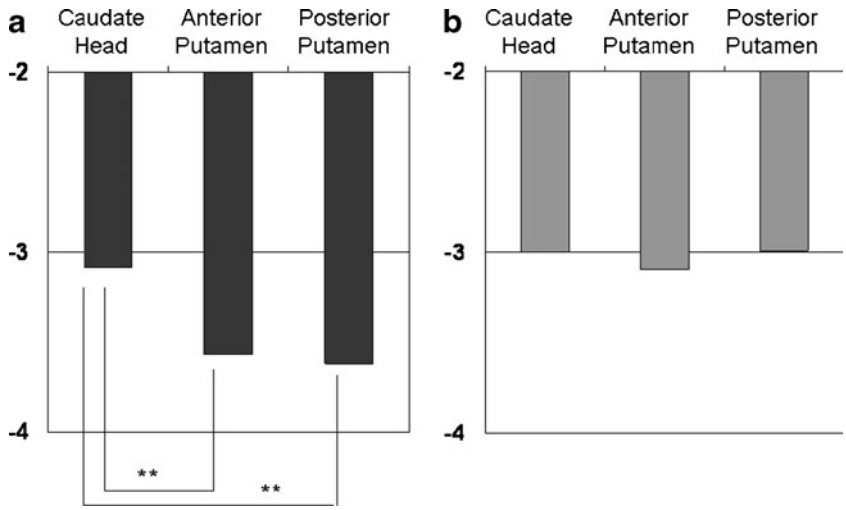

Fig. 9 Z-score of binding potentials in Parkinson's disease and Wilson's disease. **a** Z-score of participants with Parkinson's disease. **b** Z-score of participants with Wilson's disease. $^{**}p <$ 0.005, paired *t*-test

Many tracers used in dopamine receptor imaging have high specificity, leading to visual estimation as the mainstream method of analysis. However, it is very difficult to visually separate the caudate from the putamen in ^{123}I-beta-CIT SPECT images, leading instead to visual estimation of the binding potential of the whole striatum. Furthermore, visual estimation of subtle differences in uptake lead to wide variation in reference regions [7, 15]. A standard brain template may reduce these variations. The first trials of SPM and SPAM for dopamine receptor imaging began in PET scans [16]. Standard brain templates based on MRI can provide high-resolution images and objective structural differentiation. In our study, each subject image was normalized by structural matching, and their binding potentials were obtained using a template derived from standard MNI SPAM. This method reduced observer error and yielded superb reproducibility.

In a recently published study about automated analysis for dopamine receptor imaging, suboptimal VOI positioning occurred in nearly half the cases [17]. In contrast, our use of SPM with the MNI SPAM template may have resulted in proper structural normalization.

In conclusion, automated analysis of ^{123}I-beta-CIT SPECT images using SPM and SPAM was successful for participants with PD, WD, and normal controls. Our methods found significantly decreased striatal binding potential in both WD and PD compared to normal controls. We further elucidated differences in regional binding potential between PD and WD by obtaining the regional binding potential of each subject. Using this automated method, we achieved an accurate and objective quantitative analysis of dopamine receptor images.

Conflict of interest None

References

1. Mazziotta JC, Toga AW, Evans A, Fox P, Lancaster J. A probabilistic atlas of the human brain: theory and rationale for its development. The International Consortium for Brain Mapping (ICBM). Neuroimage. 1995;2(2):89–101.
2. Lee H-Y, Paeng JC, Lee DS, Lee JS, Oh CW, Cho MJ, et al. Efficacy assessment of cerebral arterial bypass surgery using statistical parametric mapping and probabilistic brain atlas on basal/acetazolamide brain perfusion SPECT. J Nucl Med. 2004;45(2):202–6.
3. Sawamoto N, Piccini P, Hotton G, Pavese N, Thielemans K, Brooks DJ. Cognitive deficits and striato-frontal dopamine release in Parkinson's disease. Brain. 2008;131(Pt 5):1294–302.
4. Bernow N, Yakushev I, Landvogt C, Buchholz H-G, Smolka MN, Bartenstein P, et al. Dopamine D2/D3 receptor availability and venturesomeness. Psychiatry Res. 2011;193(2):80–4.
5. Lee T-H, Kim S-J, Kim I-J, Kim Y-K, Kim D-S, Park K-P. Statistical parametric mapping and statistical probabilistic anatomical mapping analyses of basal/acetazolamide Tc-99m ECD brain SPECT for efficacy assessment of endovascular stent placement for middle cerebral artery stenosis. Neuroradiology. 2007;49(4):289–98.
6. Joshi S, Davis B, Jomier M, Gerig G. Unbiased diffeomorphic atlas construction for computational anatomy. Neuroimage. 2004;23 Suppl 1:S151–60.
7. Jeon B, Kim JM, Jeong JM, Kim KM, Chang YS, Lee DS, et al. Dopamine transporter imaging with [123I]-beta-CIT demonstrates presynaptic nigrostriatal dopaminergic damage in Wilson's disease. J Neurol Neurosurg Psychiatr. 1998;65(1):60–4.
8. Kim Y, Im H-J, Paeng JC, Lee JS, Eo JS, Kim DH, et al. Validation of simple quantification methods for 18F-FP-CIT PET using automatic delineation of volumes of interest based on statistical probabilistic anatomical mapping and isocontour margin setting. Nucl Med Mol Imaging. 2012;46(4):254–60.
9. Shin K-H, Park S-A, Kim S-Y, Lee SJ, Oh SJ, Kim JS. Effect of animal condition and fluvoxamine on the result of [18F]N-3-fluoropropyl-2β-carbomethoxy-3β-(4-iodophenyl) Nortropane ([18F]FP-CIT) PET study in mice. Nucl Med Mol Imaging. 2012;46(1):27–33.
10. Nocker M, Seppi K, Donnemiller E, Virgolini I, Wenning GK, Poewe W, et al. Progression of dopamine transporter decline in patients with the Parkinson variant of multiple system atrophy: a voxel-based analysis of [123I]β-CIT SPECT. Eur J Nucl Med Mol Imaging. 2012;39(6):1012–20.

11. Van Dyck CH, Seibyl JP, Malison RT, Laruelle M, Wallace E, Zoghbi SS, et al. Age-related decline in striatal dopamine transporter binding with iodine-123-beta-CITSPECT. J Nucl Med. 1995;36(7):1175–81.
12. Barthel H, Sorger D, Kühn HJ, Wagner A, Kluge R, Hermann W. Differential alteration of the nigrostriatal dopaminergic system in Wilson's disease investigated with [123I]ss-CIT and high-resolution SPET. Eur J Nucl Med. 2001;28(11):1656–63.
13. Ichise M, Kim YJ, Erami SS, Ballinger JR, Vines D, Tanaka F, et al. Functional morphometry of the striatum in Parkinson's disease on three-dimensional surface display of 123I-beta-CIT SPECT data. J Nucl Med. 1999;40(4):530–8.
14. Seibyl JP, Marek KL, Quinlan D, Sheff K, Zoghbi S, Zea-Ponce Y, et al. Decreased single-photon emission computed tomographic [123I]beta-CIT striatal uptake correlates with symptom severity in Parkinson's disease. Ann Neurol. 1995;38(4):589–98.
15. Kim SE, Choi JY, Choe YS, Choi Y, Lee WY. Serotonin transporters in the midbrain of Parkinson's disease patients: a study with 123I-beta-CIT SPECT. J Nucl Med. 2003;44(6):870–6.
16. Lucignani G, Gobbo C, Moresco RM, Antonini A, Panzacchi A, Bonaldi L, et al. The feasibility of statistical parametric mapping for the analysis of positron emission tomography studies using 11C-2-beta-carbomethoxy-3-beta-(4-fluorophenyl)-tropane in patients with movement disorders. Nucl Med Commun. 2002;23(11):1047–55.
17. Koch W, Radau PE, Hamann C, Tatsch K. Clinical testing of an optimized software solution for an automated, observer-independent evaluation of dopamine transporter SPECT Studies. J Nucl Med. 2005;46(7):1109–18.